Automatically generated rough PDF by ProofCheck from River Valley Technologies Ltd

Viktor Sverdlov<sup>1</sup> / Dmitri Osintsev<sup>1</sup> / Siegfried Selberherr<sup>1</sup>

# Silicon-on-insulator for spintronic applications: spin lifetime and electric spin manipulation

<sup>1</sup> Institute for Microelectronics, TU Wien, Gußhausstraße 27–29/E360, A-1040 Wien, Austria, E-mail: iue.tuwien.ac.at, iue.tuwien.ac.at, selberherr@iue.tuwien.ac.at

#### Abstract

With complementary metal-oxide semiconductor feature size rapidly approaching ultimate scaling limits, the electron spin attracts much attention as an alternative to the electron charge degree of freedom for low-power reprogrammable logic and nonvolatile memory applications. Silicon, the main element of microelectronics, appears to be the perfect material for spin-driven applications. Despite an impressive progress in understanding spin properties in metal-oxide-semiconductor field-effect transistors (MOSFETs), spin manipulation in a silicon channel by means of the electric field-dependent Rashba-like spin-orbit interaction requires channels much longer than 20 nm channel length of modern MOSFETs. Although a successful realization of the spin field-effect transistor seems to be unlikely without a new concept for an efficient way of spin manipulation in silicon by purely electrical means, it is demonstrated that shear strain dramatically reduces the spin relaxation, thus boosting the spin lifetime by an order of magnitude. Spin lifetime enhancement is achieved by lifting the degeneracy between the otherwise equivalent unprimedsubbands by [110] uniaxial stress. The spin lifetime in stressed ultra-thin body silicon-on-insulator structures can reach values close to those in bulk silicon. Therefore, stressed silicon-on-insulator structures have a potential for spin interconnects.

**Keywords:** Ultra-thin body SOI, shear strain, spin–orbit interaction, inter- and intravalley scattering, spin relaxation, spin lifetime enhancement, spin field-effect transistor, tunneling magnetoresistance

**DOI:** 10.1515/psr-2016-0009

### 1 Introduction

Continuous miniaturization of complementary metal-oxide semiconductor (CMOS) devices has made possible a tremendous increase in performance, speed, and density of modern integrated circuits. Numerous outstanding technological challenges have been resolved on this exciting journey. Among the most crucial technological changes recently adopted by the semiconductor industry was the introduction of a new type of multigate three-dimensional (3D) transistors [1]. This technology, combined with strain techniques and high-k dielectrics/metal gates, offers great performance and power advantages over the planar structures and allows continuous scaling down to 14 nm feature size [2]. There are good indications that device miniaturization with some technological adaptations will continue its pace down to the 10-nm technology node. A multigate 3D device architecture potentially allows device scaling beyond 10 nm, where transport in the channel is supposed to become nearly ballistic. However, even though the transistor size is scaled down, the load capacitance per unit area of a circuit stops decreasing. This suggests that the on-current must stay constant in order to maintain appropriate high-speed operation, which clearly puts limitations to the continuation of the increase in the performance of integrated circuits, and the need for research to find alternative technologies and computational principles becomes urgent. The principle of metal-oxide-semiconductor field-effect transistor (MOSFET) operation is fundamentally based on the charge degree of freedom of an electron: The electron charge interacts with the gate-induced electric field, which can close the transistor by creating a potential barrier. Another intrinsic electron property, the electron spin, attracts at present much attention as a possible candidate for complimenting or even replacing the charge degree of freedom in future electron devices [3, 4]. The electron spin state is characterized by one of the two of its possible projections on a given axis and could be potentially used in digital information processing. In addition, it takes an amazingly small amount of energy to invert the spin orientation, which is necessary for low-power applications. Even more, the electron spin as a vector may be pointed not only up or down but rather in any direction on a unit Bloch sphere. This opens the way to use the whole Bloch sphere of states to process and store information by initializing, manipulating, and detecting the

Automatically generated rough PDF by ProofCheck from River Valley Technologies Ltd

spin orientation. Because the electron spin is a purely quantum mechanical object, the set of states on a Bloch sphere is called a *quantum bit*, ora *qubit*, as opposed to a bit of classical binary information.

A quantum computer uses qubits for information processing. Due to their quantum mechanical nature, several qubits could form a superposition and be in an entangled state. The initially proposed quantum computation scheme [5] was based on spins in quantum dots. A successful implementation of spins based on quantum computer requires the possibility of efficient spin initiation, coherent manipulation, and reliable readout. An unprecedented advantage in these fields has been achieved by the researchers in the last decade [6]. The experiments on electron spins in semiconductors were performed at cryogenic temperatures, where a relaxation time of several seconds in silicon was demonstrated [7]. Although these results are encouraging, the development of a robust two-qubit gate becomes a pressing challenge [8] before proceeding to a larger computational network.

Until recently, silicon, the main material used by modern microelectronics, was remaining aside from the main stream of spin-related applications. Certainly, the use of silicon for spin-driven devices will greatly facilitate their integration with MOSFETs on the same chip. In addition, silicon possesses several unique properties extremely attractive for spin-driven applications. It is predominantly composed of nuclei of the <sup>28</sup>Si isotope without magnetic moment, which favors longer spin lifetime. Another source of spin relaxation, the spin-orbit interaction, is also weak in silicon. Because of these properties, electron spin states of conduction electrons in silicon should show better stability and lower decoherence, which make silicon a perfect candidate for spin-driven device applications. Although it should be straightforward to inject spin-polarized carriers into silicon from a ferromagnetic contact, due to a fundamental conductivity mismatch problem [9] between a ferromagnetic metal contact and the semiconductor, the problem was without solution for a long time. A special technique [10] based on the attenuation of hot electrons with spins antiparallel to the magnetization of the ferromagnetic film allowed creating an imbalance between the electrons with spin up and spin down in silicon, thus injecting spin-polarized current. The spin-coherent transport through the device was studied by applying an external magnetic field, causing precession of spins during their propagation from source to drain. The detection is performed with a similar hot electron spin filter. Although the drain current is fairly small due to the carriers' attenuation in the source and drain filters as compared to the current of injected spins, the experimental setup represents a first spin-driven device, which can be envisaged working at room temperature. Contrary to the MOSFET, however, the described structure is a two-terminal device. Nevertheless, the first demonstration of coherent spin transport through an undoped 350 µm thick silicon wafer [11] has triggered a systematic study of spin transport properties in silicon [12].

# 2 Silicon spin field-effect transistor

The spin field-effect transistor (SpinFET) is a future semiconductor spintronic device promising a performance superior to what can be achieved with the present transistor technology. SpinFETs are composed of two ferromagnetic contacts (source and drain), linked by a nonmagnetic semiconductor channel region. The ferromagnetic contacts inject and detect spin-polarized electrons, analogous to polarizer and analyzer as indicated already long ago by Datta and Das [13]. Because of the effective spin-orbit interaction into the channel, which depends on the perpendicular effective electric field, the spin of an electron injected from the source starts precessing. In order to distinguish this electric field-dependent spin-orbit interaction acting on any electron moving in a crystal potential, we term the electric field-dependent spin-orbit interaction as *coupling*. The electrons with spin, or, to be more precise, with the direction of the magnetic moment, aligned to the drain magnetization direction can easily leave the channel to the drain, thus contributing to the current. The total current through the device depends on the relative angle between the magnetization direction of the drain contact playing the role of an analyzer and the electron spin polarization at the end of the semiconductor channel. An additional current modulation is achieved by tuning the strength of the spin-orbit interaction in the semiconductor region, which depends on the effective electric field and can be controlled by purely electrical means by applying a gate voltage.

Although the SpinFET was proposed two decades ago [13], it has not been experimentally demonstrated up to now. In order to realize the SpinFET, the following requirements must be fulfilled [14]. First, an efficient spin injection in the channel (and detection) must be realized. Second, because the electron spin in the channel is not a conserved quantity and thus relaxes due to spin-flip processes, the corresponding scattering mechanisms must be detected and analyzed. It is important to identify the possibilities compatible with modern MOSFET technology, which can enhance the spin lifetime and spin diffusion length in the silicon channel. Finally, purely electrical means of spin manipulation in the channel must be identified to control the spin and thus the current flow to the drain. An example of such a manipulation is the gate voltage–dependent effective spin–orbit inter-

Automatically generated rough PDF by *ProofCheck* from River Valley Technologies Ltd

action defining the degree of the spin precession. Next we briefly discuss recent achievements and challenges for the practical realization of the SpinFET.

Spin injection into silicon and other semiconductors by purely electrical means from a ferromagnetic metal electrode was not very successful until recently. The fundamental reason has been identified as an impedance mismatch problem [9]. Even though there is a large spin imbalance between the majority and minority spins in a metal ferromagnet, both channels with spin up and spin down are equally populated in a semiconductor due to the relatively small density of states as compared to that for the minority spins in a ferromagnet. In other words, because of the large resistance of the semiconductor, the voltage applied to the contact between the ferromagnet and the semiconductor drops completely within the semiconductor. Therefore, the properties of the contact are dominated by the nonmagnetic semiconductor, thus resulting in a current without spin polarization. One solution to overcome the impedance mismatch problem is the use of hot electron injection [10]; however, the efficiency of spin injection and detection is very limited. Another solution to the impedance mismatch problem is the introduction of a potential barrier between the metal ferromagnet and the semiconductor [15]. In this case the influx of carriers from the ferromagnet into the semiconductor is reduced to such an extent that the majority spins supply just enough carriers to support the complete occupancy of the corresponding states in the semiconductor. Under such conditions the minority spin flow in semiconductors will be a fraction of that for the majority spins defined by the spin polarization in the ferromagnet. This guarantees the existence of a spin-polarized current and the spin injection into the semiconductor.

A successful experimental proof of spin injection at low temperature from an iron electrode through Al<sub>2</sub>O<sub>3</sub> [16, 17] was demonstrated only in 2007. At room temperature spin injection into silicon was first demonstrated in 2009 [18]. The authors took heavily doped silicon samples to avoid an extended depletion layer causing large tunnel barriers. It was actually this depletion layer, not the impedance mismatch problem, that prevented for a long time all the successful electrical demonstration of spin injection into silicon. It then follows that the tunnel contacts have to be optimized in order to facilitate spin injection: They must not be too thick to make the signal observable, but at the same time they must not be too transparent to avoid the impedance mismatch problem [12, 19]. Recently, tunnel contacts made of single-layer graphene [20] have been shown to deliver a contact resistance close to the optimum [21]. Electrical spin injection through silicon dioxide at temperatures as high as 500 K has also been demonstrated [22]. The tunnel barrier in the contact of a ferromagnet to a semiconductor introduces spin-dependent interface resistances [12], defining the tunnel spin polarization. Due to the additional spinfiltering effect in MgO, the high-quality tunneling stack made of a Fe and MgO (001) crystalline barrier is expected to provide spin polarization up to 70% at room temperature [23]. Spin injection using MgO dielectric as a tunnel junction has been successfully demonstrated at room temperature [24, 25]. Currently, a reliable injection of spin into doped silicon has been demonstrated from a number of ferromagnetic electrodes through several dielectric tunnel barriers. Regardless of an ultimate success in demonstrating spin injection into silicon at room temperature, there are unsolved challenges that may put the results obtained in question or even compromise our present understanding of the spin injection process in general.

There exists a several orders of magnitude discrepancy between the signal measured and the theoretical value [12]. The reasons for the discrepancies are heavily debated [12, 26, 27], and it is apparent that more research is needed to resolve this controversy. Spin can be injected into silicon by other techniques as well. The injection of spins by heat [28] is one of them, for which a spin current through the contact exists without a charge current. Another technique is spin charge pumping by inducing magnetic excitations in a material that is in contact with a semiconductor [29]. This technique is free of the impedance mismatch problem and can generate pure spin currents at room temperature [30]. The magnons are excited by the microwave. Although this technique is extremely useful to demonstrate spin injection and study spin transport in semiconductors, it remains to be seen if it is efficient enough for device applications [31]. The use of ferromagnetic contacts made of semiconductors would be another possible solution to the impedance mismatch problem. Unfortunately, no semiconductors with ferromagnetic properties surviving up to room temperature are known [32]. Another solution to resolve the impedance mismatch problem is to use half-metallic ferromagnets [33].

For the functionality of the Datta–Das SpinFET, the possibility to transfer the excess spin injected from the source to the drain electrode is essential. The excess spin is not a conserved quantity: While diffusing, it gradually relaxes to its equilibrium value, which is zero in a nonmagnetic semiconductor. It was demonstrated that spin can propagate through a 350-µm silicon wafer at liquid nitrogen temperatures. The lower estimation for the spin lifetime at room temperature obtained within the three-terminal injection scheme is of the order 0.1–1 ns [12]. The spin lifetime is determined by the spin-flip processes. Several important spin relaxation mechanisms are identified [3, 4]. In silicon at elevated temperatures the spin relaxation due to the Elliot–Yafet mechanism [3, 4] becomes important. The Elliot–Yafet mechanism is mediated by the intrinsic interaction between the orbital motion of an electron and its spin. Due to the spin dependence, the microscopic spin–orbit interaction does not conserve the electron spin; thus it generates spin flips, which is the Yafet process. When the microscopic spin– orbit interaction is taken into account, the Bloch function with a fixed spin projection is

not an eigenfunction of the total Hamiltonian. Because the eigenfunction always contains a contribution with an opposite spin projection, even spin-independent scattering with phonons generates a small probability of spin flips, which is the Elliot process. A good agreement between the experimentally observed and calculated spin lifetime as a function of temperature has been achieved, confirming that in bulk silicon the Elliot– Yafet mechanism is the dominant spin relaxation mechanism at ambient temperatures [34]. The main contribution to the spin relaxation was identified to be optical phonon scattering between the valleys residing at different crystallographic axis or f-phonon scattering [35, 36]. The intervalley scattering gets enhanced at high electric fields due to the accelerated f-phonon emission process [37], which results in an unusual behavior, when the reduction of the carrier transition time between the injector and the collector is accompanied by a contraction of spin polarization.

However, a relatively large spin relaxation experimentally observed in electrically gated lateral-channel silicon structures [38, 39] indicates that the extrinsic interface-induced spin relaxation mechanism becomes important. This may pose an obstacle in realizing spin-driven CMOS-compatible devices, and a deeper understanding of fundamental spin relaxation mechanisms in silicon inversion layers, thin films, and fins is needed. The theory of spin relaxation must account for the most relevant scattering mechanisms that are due to electron–phonon interaction and surface roughness (SR) scattering. In order to evaluate the corresponding scattering matrix elements, the wave functions must be provided. To find the wave functions, an approach based on an effective  $k \cdot p$  Hamiltonian appears to be rigorous enough to capture the most important physics while still allowing to keep the computational efforts bearable. The effective  $k \cdot p$  Hamiltonian must include the effective spin–orbit interaction [35], which, apart from scattering, is the main ingredient of the Elliot–Yafet spin relaxation mechanism. In addition, the confinement potential is included. It is also desirable to have other effects such as a sufficiently accurate model of the conduction band valley, nonparabolicity and warping, and external stress [40] incorporated.

## 3 Subband wave functions in silicon-on-insulator structures

The conduction band of bulk silicon consists of three pairs of valleys near the edges of the Brillouin zone along the [100], [010], and [001] crystallographic axes. Each state is described by the valley index, the wave vector k, and the spin orientation (spin up and spin down) on a chosen axis. The Hamiltonian satisfying all the requirements listed earlier is written in the vicinity of the X-point of the Brillouin zone. It considers the two closest to the X-point valleys described by the basic functions  $X_1$  and  $X_2$  augmented with the two possible spin projections: $X_{1\uparrow}$ ,  $X_{1\downarrow}$ ,  $X_{2\uparrow}$ , where  $\uparrow$  and  $\downarrow$  indicate the spin projection at the quantization z-axis. The Hamiltonian of the valley pairs along the [001]-axis is then given as [41]

$$H = \begin{bmatrix} H_1 & H_3 \\ H_3^{\dagger} & H_2 \end{bmatrix} \tag{1}$$

with  $H_1$ ,  $H_2$ , and  $H_3$  defined as

$$H_1 = \left[ \frac{\hbar^2 k_z^2}{2m_l} - \frac{\hbar^2 k_0 k_z}{m_l} + \frac{\hbar^2 (k_x^2 + k_y^2)}{2m_t} + U(z) \right] I, \tag{2}$$

$$H_2 = \left[ \frac{\hbar^2 k_z^2}{2m_l} - \frac{\hbar^2 k_0 k_z}{m_l} + \frac{\hbar^2 (k_x^2 + k_y^2)}{2m_t} + U(z) \right] I, \tag{3}$$

$$H_{3} = \begin{bmatrix} D\varepsilon_{xy} - \frac{\hbar^{2}k_{x}k_{y}}{M} & (k_{y} - k_{x}i)\Delta_{So} \\ (-k_{y} - k_{x}i)\Delta_{SO} & D\varepsilon_{xy} - \frac{\hbar^{2}k_{x}k_{y}}{M} \end{bmatrix}.$$
 (4)

Here I is the identity  $2 \times 2$  matrix,  $m_t$  and  $m_l$  are the transversal and the longitudinal silicon effective masses,  $k_0 = 0.15 \times 2\pi/a$  is the position of the valley minimum relative to the X-point in unstrained silicon,  $\varepsilon_{xy}$  denotes the shear strain component,  $M^{-1} \approx m_t^{-1} - m_0^{-1}$ , and D = 14 eV is the shear strain deformation potential. The spin– orbit term  $\tau_y \otimes (k_x \sigma_x - k_y \sigma_y)$  with

$$\Delta_{\text{so}} = 2 \left| \sum \frac{\left\langle X_1 \left| p_j \right| n \right\rangle \left\langle n \left| \left[ \nabla V \times p \right]_j \right| X_{2'} \right\rangle}{E_n - E_X} \right|$$
 (5)

couples states with the opposite spin projections from the opposite valleys. The matrices  $\sigma_x$  and  $\sigma_y$  are the spin Pauli matrices and  $\tau_y$  is the *y*-Pauli matrix in the valley degree of freedom space. In the Hamiltonian (2.1) U(z) is the confinement potential, and the value  $\Delta_{so} = 1.27$  meV nm computed by the empirical pseudopotential method (see Figure 1) is close to the one reported by Li and Dery [35].

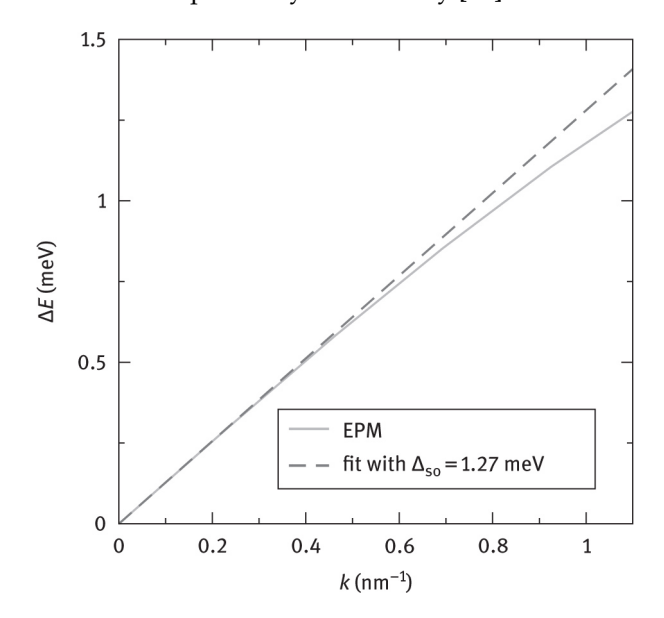


**Figure 1:** Empirical pseudopotential calculations of the spin–orbit interaction strength by evaluating the gap opening at the *X*-point between  $X_1$  and  $X_2$ ' for finite  $k_x$ .

In the presence of strain and confinement, the fourfold degeneracy of the n-th unprimed subband is partly lifted by forming an n+ and n- subladders (the valley splitting); however, the degeneracy of the eigenstates with the opposite spin projections  $n \pm \uparrow$  and  $n \pm \downarrow$  within each subladder is preserved.

The degenerate states are chosen to satisfy

$$\langle \uparrow n \pm | f | n \pm \downarrow \rangle = 0 \tag{6}$$

with the operator f defined as

$$f = \cos\theta \,\sigma_z + \sin\theta \,(\cos\varphi \,\sigma_x + \sin\varphi \,\sigma_y),\tag{7}$$

where  $\theta$  is the polar and  $\varphi$  is the azimuth angle defining the orientation of the injected spin. In general, the expectation value of the operator f computed between the spin-up and spin-down states from different subladders is nonzero, when the effective magnetic field direction due to the spin-orbit interaction is different from the injected spin quantization axis.

$$f = \langle \uparrow n + | f | n + \downarrow \rangle \neq 0 \tag{8}$$

The Hamiltonian (2.1) is suitable for describing unprimed subbands in (001) thin silicon films. If the confinement is strong, the primed subbands lying higher in energy because of a much smaller quantization mass  $m_{\rm t}$  are disregarded, and all the properties including low field transport and spin relaxation can be evaluated with the help of the wave functions of the lowest unprimed subbands evaluated with Eqn. (1). In the case when the confinement potential is approximated with an infinite square well, the unprimed subband energy difference can be approximated as [41]:

$$\Delta E_n = \frac{2y_n^2 B}{k_0 t \sqrt{(1 - y_n^2 - \eta^2)(1 - y_n^2)}} \left| \sin \left( \sqrt{\frac{1 - y_n^2 - \eta^2}{1 - y_n^2}} k_0 t \right) \right|$$
(9)

 $y_n$ ,  $\eta$ , and B are defined as

$$y_n = \frac{\pi n}{k_0 t},\tag{10}$$

$$\eta = \frac{m_l B}{\hbar^2 k_0^2},\tag{11}$$

and

$$B = \sqrt{\Delta_{\text{so}}^2(k_x^2 + k_y^2) + \left(D\varepsilon_{xy} - \frac{\hbar^2 k_x k_y}{M}\right)^2}.$$
 (12)

Here t is the film thickness. To obtain Eqn. (9) we have generalized the theory [42] for valley splitting by including spin-orbit coupling. It is interesting to note that because the spin-orbit interaction provides coupling between the states with the opposite spin projections but from the opposite valleys, the spin-orbit coupling term in Eqn. (9) also leads to a subband splitting in the presence of a confining potential. However, because two possible ways of coupling the state with spin-up (down) from one valley to the spin-down (up) state in the opposite valley are allowed, the double-spin degeneracy of the eigenstates is not lifted. The spin degeneracy is preserved in a general case for arbitrary momentum, when shear strain is introduced. A linear combination of these two degenerate states with opposite spin projections allows creating the wave function with a spin projection up or down on any arbitrarily chosen axis. It is usually assumed that because the unprimed subbands are originating from the two equivalent [001] valleys, they are double degenerate [43]. However, this is true only in the parabolic band approximation when the two valleys are independent. Due to the presence of the off-diagonal terms, the Hamiltonian (2.1) couples the [001] valleys, resulting in the unprimed subband degeneracy lifting described by Eqn. (9). The degeneracy between the subbands is exactly recovered, when the oscillating term is zero. However, this degeneracy is insignificant, because it does not result in any peculiar behavior of the spin relaxation scattering matrix elements. In contrast, the minimum of the B term in Eqn. (9) reveals a very strong increase of the intersubband spin relaxation. Under these conditions the subband splitting is purely determined by the linear dependence on the effective spin-orbit interaction. This linear dependence of the splitting is similar to the Zeeman splitting in a magnetic field. Thus, the spin-orbit-induced splitting can be interpreted as an effective magnetic field, while the pairs of states  $X_{1\uparrow}$ ,  $X_{2\downarrow}$  and  $X_{1\downarrow}$ ,  $X_{2\uparrow}$  it couples have similarities with the Zeeman spin-up and spin-down states split because of the effective field. Spin along the z-direction starts precessions in the in-plane effective field, resulting in a large mixing between the opposite spin states from the different valleys. This mixing results in large spin relaxation matrix elements defining hot spin relaxation spots. These hot spots should be contrasted against the hot spots in bulk silicon [35] appearing at the edge of the 3D Brillouin zone. The origin of the spin relaxation hot spots in thin films lies in the unprimed subband degeneracy in a confined electron system. Because the hot spots are determined by the minimum of Eqn. (12), they are located in the middle of the two-dimensional Brillouin zone in an unstrained film, thus contributing strongly to the spin relaxation. However, when shear strain is applied, the spin relaxation hot spots are pushed toward higher energies. Moving the hot spots above the Fermi energy outside the occupied states region will result in reduced spin relaxation and an increase of the spin lifetime with shear strain.

# Analytical evaluation of the wave functions

Because spin hotspots determine the strong dependence of the spin relaxation scattering matrix elements on the relative angle between the incoming and scattered waves, the assumption of the independence of the subband wave functions on the in-plane momentum frequently employed to estimate the momentum relaxation cannot be used to evaluate the spin lifetime. Indeed, because spin-orbit effects are linear in in-plane momentum, the calculation of the SR scattering matrix elements at the center of the 2D Brillouin zone usually done for mobility calculations would result in the complete loss of all the effects due to spin-orbit interaction. Therefore, to accurately compute the spin lifetime numerically, one needs to know the subband wave functions as a function of the in-plane wave vector. Numerical evaluation of the wave functions with subsequent integrations makes the task prohibitively expensive. To simplify the problem, we obtain the wave functions in a semianalytical manner. For this purpose we rotate the Hamiltonian (2.1) by means of the following unitary transformation. The four (13–20) with  $tan(\Theta) = \frac{\Delta_{so}\sqrt{k_x^2 + k_y^2}}{D\varepsilon_{xy} - \frac{\hbar^2 k_x k_y}{M}}$ . The transformation effectively decouples the spins with opposite direction in different values. basic functions  $X_{1\uparrow}$ ,  $X_{1\downarrow}$ ,  $X_{2\uparrow}$ ,  $X_{2\rightarrow}$  for the two [001] valleys with spin up, spin down are transformed by Eqns.

$$\psi_1 = \frac{1}{2} \left[ (X_{1\uparrow} + X'_{2\uparrow}) + (X_{1\downarrow} + X'_{2\downarrow}) \frac{k_x - ik_y}{\sqrt{k_x^2 + k_y^2}} \right]$$
 (13)

in different valleys.

$$\psi_2 = \frac{1}{2} \left[ (X_{1\uparrow} + X'_{2\uparrow}) - (X_{1\downarrow} + X'_{2\downarrow}) \frac{k_x - ik_y}{\sqrt{k_x^2 + k_y^2}} \right]$$
 (14)

$$\psi_3 = \frac{1}{2} \left[ (X_{1\uparrow} + X'_{2\uparrow}) + (X_{1\downarrow} + X'_{2\downarrow}) \frac{k_x - ik_y}{\sqrt{k_x^2 + k_y^2}} \right]$$
 (15)

$$\psi_4 = \frac{1}{2} \left[ (X_{1\uparrow} + X'_{2\uparrow}) - (X_{1\downarrow} + X'_{2\downarrow}) \frac{k_x - ik_y}{\sqrt{k_x^2 + k_y^2}} \right]$$
 (16)

$$X_1 = \psi_1 \cos\left(\frac{\Theta}{2}\right) - i\psi_3 \sin\left(\frac{\Theta}{2}\right) \tag{17}$$

$$X_2 = \psi_2 \cos\left(\frac{\Theta}{2}\right) + i\psi_4 \sin\left(\frac{\Theta}{2}\right) \tag{18}$$

$$X_3 = \psi_3 \cos\left(\frac{\Theta}{2}\right) - i\psi_1 \sin\left(\frac{\Theta}{2}\right) \tag{19}$$

$$X_4 = \psi_4 \cos\left(\frac{\Theta}{2}\right) + i\psi_2 \sin\left(\frac{\Theta}{2}\right) \tag{20}$$

The Hamiltonian (2.1) can be cast into a form in which spins with opposite orientations in different valleys are independent.

$$H = \begin{bmatrix} H_1 & H_3 \\ H_3 & H_2 \end{bmatrix} \tag{21}$$

 $H_1$ ,  $H_2$ , and  $H_3$  are written as:

$$H_1 = \left[ \frac{\hbar^2 k_z^2}{2m_l} + \frac{\hbar^2 (k_x^2 + k_y^2)}{2m_t} - \delta + U(z) \right] I, \tag{22}$$

$$H_2 = \left[ \frac{\hbar^2 k_z^2}{2m_l} + \frac{\hbar^2 (k_x^2 + k_y^2)}{2m_t} - \delta + U(z) \right] I, \tag{23}$$

$$H_3 = \begin{bmatrix} \frac{h^2 k_0 k_z}{m_I} & 0\\ 0 & \frac{h^2 k_0 k_z}{m_I} \end{bmatrix} \tag{24}$$

with 
$$\delta = \sqrt{\left(D\varepsilon_{xy} - \frac{\hbar^2 k_x k_y}{M}\right)^2 + \Delta_{SO}^2(k_x^2 + k_y^2)}$$
.

The wave functions for the Hamiltonian (22–24) can be found in a closed form [42]. This significantly simplifies the computation of the spin relaxation and momentum scattering matrix elements; relaxation and scattering rates; and, finally, the spin relaxation time and the electron mobility. Next we outline the procedure for evaluating the electron spin relaxation.

# 5 Spin relaxation suppression in stressed silicon films

We are considering three mechanisms that contribute to the spin and momentum relaxation: SR and intra- and intervalley (for spin relaxation) scattering by acoustic phonons.

The spin and momentum relaxation times are calculated by thermal averaging [35, 36, 43] as:

$$\frac{1}{\tau} = \frac{\int \frac{1}{\tau(K_1)} f(\varepsilon) (1 - f(\varepsilon)) dK_1}{\int_0^f (\varepsilon) dK_1,}$$
 (25)

$$\int dK_1 = \int_0^{2\pi} \int_0^{\infty} \frac{|K_1|}{\left|\frac{\partial \varepsilon(K_1)}{\partial K_1}\right|} d\varphi \, d\varepsilon. \tag{26}$$

The SR momentum (spin) relaxation rate is calculated in the following way:

$$\frac{1}{\tau_{SR}(K_{1})} = \frac{2(4)\pi}{\hbar(2\pi)^{2}} \sum_{i,j} \int_{0}^{2\pi} \pi \Delta^{2} L^{2} \frac{1}{\varepsilon_{ij}^{2}(K_{2} - K_{1})} \frac{\hbar^{4}}{4m_{l}^{2}} \frac{|K_{2}|}{\left|\frac{\partial \varepsilon(K_{2})}{\partial K_{2}}\right|}.$$

$$\cdot \left[ \left(\frac{d\psi_{iK_{1}\sigma}}{dz}\right)^{*} \frac{d\psi_{jK_{2}-\sigma}}{dz} \right]_{z=\pm\frac{t}{2}}^{2} \exp\left(\frac{-(K_{2} - K_{1})^{2}L^{2}}{4}\right) d\varphi, \tag{27}$$

 $\varepsilon$  is the electron energy,  $K_{1,2}$  are the in-plane wave vectors before and after scattering,  $\varepsilon_{ij}$  is the dielectric permittivity, L is the autocorrelation length,  $\Delta$  is the mean square value of the SR fluctuations,  $\Psi_{iK_1}$  and  $\Psi_{jK_2}$  are the wave functions, and  $f(\varepsilon)$  is the Fermi function, and  $\sigma$  ¼ p1 is the spin projection to the [001] axis.

The momentum relaxation time is evaluated in the standard way [44]. The spin relaxation rate due to the transversal acoustic phonons is calculated as

$$\frac{1}{\tau_{\text{TA}}(K_{1})} = \frac{4\pi k_{B}T}{\hbar\rho\nu_{\text{TA}}^{2}} \sum \int_{0}^{2\pi} \frac{|K_{2}|}{\left|\frac{\partial\varepsilon(K_{2})}{\partial K_{2}}\right|} \left[1 - \frac{\frac{\partial\varepsilon(K_{2})}{\partial K_{2}}f(\varepsilon(K_{2}))}{\frac{\partial\varepsilon(K_{1})}{\partial K_{1}}f(\varepsilon(K_{1}))}\right] \frac{1}{2} \int_{0}^{t} \int_{0}^{t} exp\left(-\sqrt{q_{x}^{2} + q_{y}^{2}}|z - z'|\right) \cdot \left[\Psi_{K_{2}-\sigma}^{+}(z)M\Psi_{K_{1}\sigma}(z)\right]^{*} \left[\Psi_{K_{2}-\sigma}^{+}(z')M\Psi_{K_{1}\sigma}(z')\right] \cdot \left[\sqrt{q_{x}^{2} + q_{y}^{2}} - \frac{8q_{x}^{2}q_{y}^{2} - (q_{x}^{2} + q_{y}^{2})^{2}}{q_{x}^{2} + q_{y}^{2}}|z - z'|\right] dzdz' \frac{d\varphi}{2\pi}, \tag{28}$$

where  $k_{\rm B}$  is the Boltzmann constant, T is the temperature,  $\rho=2329\frac{{\rm kg}}{{\rm m_2}}$  is the silicon density,  $v_{\rm TA}=5300\frac{{\rm m}}{{\rm s}}$  is the transversal phonons velocity,  $(q_x,q_y)={\rm K_1-K_2}$ , and M is the matrix  $4\times4$ . Written in the basis for the spin relaxation rate the matrix M is

$$M = \begin{bmatrix} 0 & 0 & \frac{D}{2} & 0\\ 0 & 0 & 0 & \frac{D}{2}\\ \frac{D}{2} & 0 & 0 & 0\\ 0 & \frac{D}{2} & 0 & 0 \end{bmatrix}. \tag{29}$$

Here D = 14 eV is the shear deformation potential.

The intravalley spin relaxation rate due to the longitudinal acoustic phonons is calculated as

$$\frac{1}{\tau_{\text{LA}}(K_{1})} = \frac{4\pi k_{B}T}{\hbar\rho\nu_{\text{LA}}^{2}} \sum \int_{0}^{2\pi} \frac{|K_{2}|}{\left|\frac{\partial\varepsilon(K_{2})}{\partial K_{2}}\right|} \left[1 - \frac{\frac{\partial\varepsilon(K_{2})}{\partial K_{2}}f(\varepsilon(K_{2}))}{\frac{\partial\varepsilon(K_{1})}{\partial K_{1}}f(\varepsilon(K_{1}))}\right] \frac{1}{2} \int_{0}^{t} \int_{0}^{t} exp\left(-\sqrt{q_{x}^{2} + q_{y}^{2}}|z - z'|\right) \cdot \left[\Psi_{K_{2}-\sigma}(z)M\Psi_{K_{1}\sigma}(z)\right] * \left[\Psi_{K_{2}-\sigma}^{\dagger}(z')M\Psi_{K_{1}\sigma}(z')\right] \cdot \frac{4q_{x}^{2}q_{y}^{2}}{\left(\sqrt{q_{x}^{2} + q_{y}^{2}}\right)^{3}} \left[\sqrt{q_{x}^{2} + q_{y}^{2}}|z - z'| + 1\right] dzdz' \frac{d\varphi}{2\pi} \tag{30}$$

Here,  $v_{LA} = 8,700 \text{ m/s}$  is the speed of the longitudinal phonons and the matrix M is defined with Eqn. (29).

The intervalley spin relaxation rate contains the Elliot and Yafet contributions [36], which are calculated in the following way:

$$\begin{split} &\frac{1}{\tau_{\mathrm{LA}}(K_{1})} = \frac{4\pi k_{\mathrm{B}}T}{\hbar\rho v_{\mathrm{LA}}^{2}} \sum \int_{0}^{2\pi} \frac{|K_{2}|}{\left|\frac{\partial \varepsilon(K_{2})}{\partial K_{2}}\right|} \left[1 - \frac{\frac{\partial \varepsilon(K_{2})}{\partial K_{2}} f(\varepsilon(K_{2}))}{\frac{\partial \varepsilon(K_{1})}{\partial K_{1}} f(\varepsilon(K_{1}))}\right]. \\ &\cdot \frac{1}{2} \int_{0}^{t} \left[\psi_{K_{2}-\sigma}^{\dagger}(z)M'\psi_{K_{1}\sigma}(z)\right]^{*} \left[\psi_{K_{2}-\sigma}^{\dagger}(z)M'\psi_{K_{1}\sigma}(z)\right] dz \frac{d\varphi}{2\pi}. \end{split} \tag{31}$$

The matrix M' is written as

$$M' = \begin{bmatrix} M_{ZZ} & M_{SO} \\ M_{SO}^{\dagger} & M_{ZZ} \end{bmatrix}. \tag{32}$$

$$M_{ZZ} = \begin{bmatrix} D_{ZZ} & 0\\ 0 & D_{ZZ} \end{bmatrix}. \tag{33}$$

$$M_{\rm so} = \begin{bmatrix} 0 & D_{\rm so}(r_y - ir_x) \\ D_{\rm so}(-r_y - ir_x) & 0 \end{bmatrix}.$$
 (34)

 $(r_x, r_y)$  ½  $K_1$   $\not\models K_2$ ,  $D_{ZZ}$  = 12 eV,  $D_{so}$  = 15 meV/ $k_0$ , with  $k_0$  = 0.15  $\cdot$  2 $\pi/a$  defined as the position of the valley minimum relative to the X-point in unstrained silicon [36].

A strong increase of the spin lifetime [45] is demonstrated in Figure 2 for a 2.5 nm thick film.

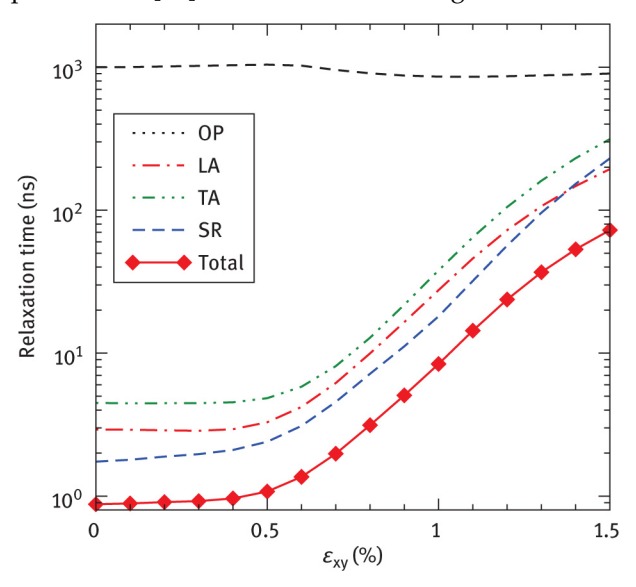


**Figure 2:** Spin relaxation time with its contributions mediated by optical phonons (OP), longitudinal acoustic (LA), and transversal acoustic (TA), as well as due to the scattering on surface roughness (SR). Film thickness is 2.5nm, room temperature.

The spin lifetime is boosted by almost two orders of magnitude. The fact that the in-plane momentum dependence of the subband wave functions must be preserved significantly increases the demands for computational resources and requires extensive code parallelization. For film thickness below 3 nm, the SR scattering mechanism dominates the spin relaxation for all electron concentration and shear strain values.

For films thicker than 3 nm, acoustic phonon–mediated spin relaxation starts playing an important role as shown in Figure 3.

Film thickness is 2.5 nm, room temperature.

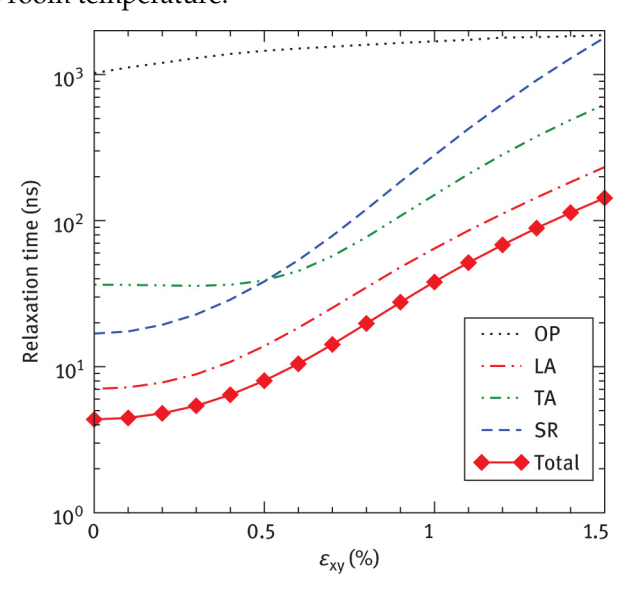


Figure 3: Spin relaxation time with its contributions in a 4 nm thick film.

Spin relaxation due to optical phonons is the weakest among the considered mechanisms. In contrast to the momentum relaxation defined by the intrasubband transitions, the main contribution to the spin relaxation comes from the intersubband scattering processes. This is due to the presence of the spin hot spots at which the spin-up and spin-down states from the unprimed subbands split by the spin-orbit interaction are strongly coupled. The position of the hot spots defined by

$$\varepsilon_{xy} = \frac{\hbar^2 \left| k_x k_y \right|}{MD} \tag{35}$$

is pushed to higher momentum states away from the subband minimum as the value of the shear strain increases. As the spin relaxation hot spots move above the Fermi level into unoccupied state region, the spin relaxation is strongly reduced, which results in a significant spin lifetime increase with shear strain applied. Interestingly, at high stress the value of the spin relaxation is comparable to that in bulk silicon. This makes silicon-on-insulator structures very attractive for spin-driven applications, in particular, for spin interconnects.

## 6 Spin manipulation in silicon FETs at room temperature

Utilizing spin properties of electrons for future microelectronic devices opens great opportunities to reduce device power consumption. As outlined earlier, the ferro-magnetic source contact injects spin-polarized electrons to the semiconductor region [13]. At the drain contact only the electrons with spin aligned to the drain magnetization can easily leave the channel and contribute to the current. Thus, the total current through the device depends on the relative angle between the magnetization direction of the drain contact and the electron spin polarization at the end of the semiconductor channel. Current modulation is achieved by tuning the strength of the spin-orbit coupling in the semiconductor region. The spin-orbit coupling is taken in the Rashba form [46, 47], with the spin-orbit coupling strength depending on the effective electric field and thus the gate voltage [46]. The electric field-dependent spin-orbit coupling splits the degeneracy between the spin-up and spin-down states moving with the same velocity in the same direction, thus opening the way to manipulate the degree of spin precession in the channel. In the absence of the spin-orbit coupling and the external magnetic field, the electrons propagate with their spin orientation conserved. The strength of the spin-orbit coupling determines the minimum length of the semiconductor channel sufficient to change the orientation of the spin to the opposite. In silicon, the spin-orbit coupling is relatively weak [48–50]. Figure 4 shows the modulation of the channel resistance in [001] oriented channel as a function of the spin-orbit coupling strength  $\beta$  for a channel with the length of  $8 \mu m$ . In order to facilitate the spin injection and detection, the tunnel barriers U between the channel and the source and drain of the dimensionless strength  $z = 2m_f^* U(2\pi/h)^2 k_F^{-1}$ , where  $m_f^*$  and  $k_F$  are the effective mass and the Fermi vector in the ferromagnetic contacts, respectively. Figure 4 demonstrates that the modulation of the resistance in the channel is preserved at room temperatures and may reach about 60%, which is sufficient for applications.

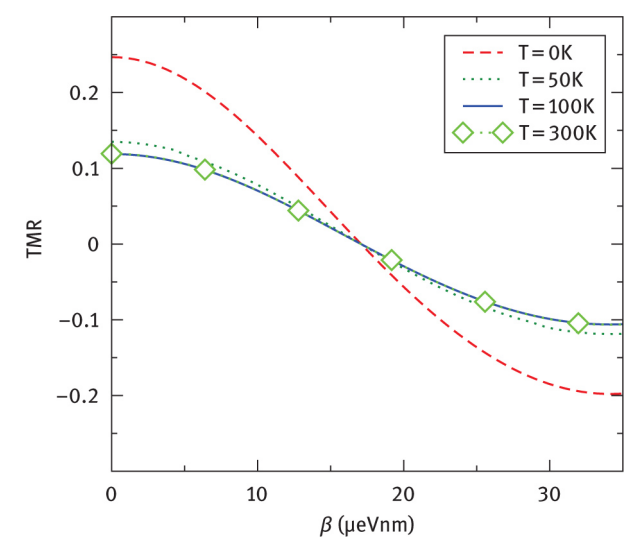


**Figure 4:** TMR dependence on the value of the Dresselhaus spin–orbit interaction for  $E_F = 2.47$  eV,  $\delta Ec = 2.154$  eV, P = 0.4, z = 3,  $t = 8 \mu m$ , V = 1 meV.

At the same time, this modulation is inferior to the maximum-reported tunneling magnetoresistence ratio of about 600% in magnetic tunnel junctions at room temperature. Due to the weak spin–orbit coupling, the channel length L should be at least

$$L = \frac{h}{\beta m_n},\tag{36}$$

where  $m_n$  is an effective mass in the silicon channel. For typical values of the spi-n- orbit coupling  $\beta$ , this value is in several microns range. This length is much longer than 20 nm channel length in modern cutting-edge MOSFET transistors. To reduce the length of a channel in a SpinFET, a much more efficient way to manipulate spins by purely electrical means is required. The remaining option to build a reprogrammable MOSFET by using ferromagnetic source and drain is still of great interest. Indeed, although magnetic tunnel junctions possess much larger ratio of tunneling magnetoresistances for parallel and antiparallel layer magnetization orientation, these are still two-terminal devices and the realization and usefulness of MOSFETs with magnetic source and drain are pending to be explored from the points of view of both technology and applications.

#### 7 Conclusion

The spin–orbit interaction effects included into the effective low-energy  $k \cdot p$  Hamiltonian allow the investigation of the valley splitting as well as momentum and spin relaxation mediated by the SR and phonon scattering in a thin-film SOI MOSFET in a wide range of parameters. To evaluate the wave function dependence on the inplane momentum and spin relaxation time, the  $k \cdot p$  Hamiltonian was solved analytically. We have demonstrated that the valley splitting minimum due to the vanishing  $D\varepsilon_{xy} - \frac{\hbar^2 k_x k_y}{M} = 0$  leads to an extremely strong spin relaxation. This is because the splitting is solely determined by the spin–orbit field strongly coupling spin-up and spin-down states from different valleys. With shear strain increased, these hot spots are pushed to high energies outside the occupied states. This results in a sharp decrease of spin relaxation and thus in a giant, almost two orders of magnitude, increase of the spin lifetime. This is in contrast to the mobility that can be improved by a factor of two. As shear strain is now routinely used to boost mobility, it is a viable option to increase the spin lifetime in ultra-thin body silicon-on-insulator structures, making them promising for future spin interconnects.

#### Acknowledgments

This work was supported by the European Research Council through the grant #247056 MOSILSPIN. The computational results are achieved on the Vienna Scientific Cluster (VSC).

This article is also available in: Liou (et al.), Nano Devices and Sensors. De Gruyter (2016), isbn 978-1-5015-1050.

## References

- [1] M. Bohr, The evolution of scaling from the homogeneous era to the heterogeneous era, in: *International Electron Devices Meeting (IEDM)*, 2011, pp. 1.1.1–1.1.6.
- [2] S. Natarajan, M. Agostinelli, S. Akbar, M. Bost, A. Bowonder, et al., A 14nm logic technology featuring 2nd-generation FinFET, air-gapped interconnects, self-aligned double patterning and a 0.0588 μSRAM cell size, in: *International Electron Devices Meeting (IEDM)*, 2014, pp. 3.7.1–3.7.3.
- [3] I. Zutic, J. Fabian, S. Das Sarma, Spintronics: Fundamentals and applications, Rev. Mod. Phys. 76 (2004) 323-410.
- [4] J. Fabian, A. Matos-Abiaguea, C. Ertler, P. Stano, I. Zutic, Semiconductor spintronics, Acta Phys. Slovaca 57 (2007) 565–907.
- [5] D. Loss, D. P. DiVincenzo, Quantum computation with quantum dots, Phys. Rev. A 57 (1998) 120-126.
- [6] F. A. Zwanenburg, A. S. Dzurak, A. Morello, M. Y. Simmons, L. C. L. Hollenberg, G. Klimeck, S. Rogge, S. N. Coppersmith, M. A. Eriksson, Silicon quantum electronics, *Rev. Mod. Phys.* 85 (2013) 961–1019.
- [7] A. Morello, J. J. Pla, F. A. Zwanenburg, K. W. Chan, K. Y. Tan, H. Huebl, M. Mottonen, C. D. Nugroho, C. Yang, J. A. van Donkelaar, A. D. C. Alves, D. N. Jamieson, C. C. Escott, L. C. L. Hollenberg, R. G. Clark, A. S. Dzurak, Single-shot readout of an electron spin in silicon, *Nature* 479 (2010) 345–353.
- [8] D. D. Awschalom, L. C. Bassett, A. S. Dzurak, E. L. Hu, J. R. Petta, Quantum spintronics: Engineering and manipulating atom-like spins in semiconductors, *Science* 339 (6124) (2013) 1174–1179.
- [9] G. Schmidt, D. Ferrand, L. W. Molenkamp, A. T. Filip, B. J. van Wees, Fundamental obstacle for electrical spin injection from a ferromagnetic metal into a diffusive semiconductor, *Phys. Rev. B* 62 (2000) R4790–R4793.

- [10] I. Appelbaum, B. Huang, D. J. Monsma, Electronic measurement and control of spin transport in silicon, Nature 447 (2007) 295–298.
- [11] B. Huang, D. J. Monsma, I. Appelbaum, Coherent spin transport through a 350 micron thick silicon wafer, Phys. Rev. Lett. 99 (2007) 177209.
- [12] R. Jansen, Silicon spintronics, Nature Materials 11 (2012) 400–408.
- [13] S. Datta, B. Das, Electronic analog of the electro-optic modulator, Appl. Phys. Lett. 56 (7) (1990) 665–667.
- [14] S. Sugahara, J. Nitta, Spin-transistor electronics: An overview and outlook, Proc. IEEE 98 (12) (2010) 2124–2154.
- [15] E. I. Rashba, Theory of electrical spin injection: Tunnel contacts as a solution of the conductivity mismatch problem, *Phys. Rev. B* 62 (2000) R16267–R16270.
- [16] B. T. Jonker, G. Kioseoglou, A. T. Hanbicki, C. H. Li, P. E. Thompson, Electrical spin-injection into silicon from a ferromagnetic metal/tunnel barrier contact, *Nature Physics* 3(2007)542–546.
- [17] O. M. J. vant Erve, A. T. Hanbicki, M. Holub, C. H. Li, C. Awo-Affouda, P. E. Thompson, B. T. Jonker, Electrical injection and detection of spin-polarized carriers in silicon in a lateral transport geometry, *Appl. Phys. Lett.* 91 (21) (2007) 212109.
- [18] S. P. Dash, S. Sharma, R. S. Patel, M. P. de Jong, R. Jansen, Electrical creation of spin polarization in silicon at room temperature, *Nature* 462 (2009) 491–494.
- [19] K. Motohashi. B.-C. Min, C. Lodder, R. Jansen, Tunable spin tunnel contacts to silicon using low-work-function ferromagnets, *Nature Materials* 5 (2006) 817–822.
- [20] O. M. J. van 't Erve, A. L. Friedman, E. Cobas, C. H. Li, J. T. Robinson, B. T. Jonker, Low-resistance spin injection into silicon using graphene tunnel barriers, *Nature Nanotechnology* 7 (2012) 737–742.
- [21] R. Jansen, S. P. Dash, S. Sharma, B. C. Min, Silicon spintronics with ferromagnetic tunnel devices, *Semiconductor Science and Technology* 27 (8) (2012) 083001.
- [22] C. Li, O. van 't Erve, B. Jonker, Electrical injection and detection of spin accumulation in silicon at 500K with magnetic metal/silicon dioxide contacts, *Nature Communications* 2 (2011) 245.
- [23] S. Yuasa, D. D. Djayaprawira, Giant tunnel magnetoresistance in magnetic tunnel junctions with a crystalline MgO (001) barrier, J. Phys. D 40 (21) (2007) R337.
- [24] K.-R. Jeon, B.-C. Min, I.-J. Shin, C.-Y. Park, H.-S. Lee, Y.-H. Jo, S.-C. Shin, Electrical spin accumulation with improved bias voltage dependence in a crystalline CoFe/MgO/Si system, *Appl. Phys. Lett.* 98 (26) (2011) 262102.
- [25] A. Spiesser, S. Sharma, H. Saito, R. Jansen, S. Yuasa, K. Ando, Electrical spin injection in p-type Si using Fe/MgO contacts, in: *Proc. SPIE*, 8461, 2012, p. 84610K.
- [26] R. Jansen, A. M. Deac, H. Saito, S. Yuasa, Injection and detection of spin in a semiconductor by tunneling via interface states, *Phys. Rev. B* 85 (2012) 134420.
- [27] Y. Song, H. Dery, Magnetic-field-modulated resonant tunneling in ferromagnetic-insulator-nonmagnetic junctions, *Phys. Rev. Lett.* 113 (2014) 047205.
- [28] J.-C. L. Breton, S. Sharma, H. Saito, S. Yuasa, R. Jansen, Thermal spin current from a ferromagnet to silicon by Seebeck spin tunnelling, *Nature* 475 (2011) 82–85.
- [29] E. Shikoh, K. Ando, K. Kubo, E. Saitoh, T. Shinjo, M. Shiraishi, Spin-pump-induced spin transport in p-type Si at room temperature, Phys. Rev. Lett. 110 (2013) 127201.
- [30] K. Ando, S. Takahashi, J. Ieda, H. Kurebayashi, T. Trypiniotis, C. H. W. Barnes, S. Maekawa, E. Saitoh, Electrically tunable spin injector free from the impedance mismatch problem, *Nature Materials* 10 (2011) 655–659.
- [31] Y. Ando, K. Ichiba, S. Yamada, E. Shikoh, T. Shinjo, K. Hamaya, M. Shiraishi, Giant enhancement of spin pumping efficiency using Fe<sub>3</sub>Si ferromagnet, *Phys. Rev. B* 88 (2013) 140406.
- [32] P. Nemec, V. Novak, N. Tesarova, E. Rozkotova, H. Reichlova, D. Butkovicova, F. Trojanek, K. Olejnik, P. Maly, R. Campion, B. Gallagher, J. Sinova, T. Jungwirth, The essential role of carefully optimized synthesis for elucidating intrinsic material properties of (Ga, Mn)As, *Nature Communications* 4 (2013) 1422.
- [33] Y. Takamura, K. Hayashi, Y. Shuto, S. Sugahara, Fabrication of high-quality Co2FeSi/SiOx Ny/ Si(100) tunnel contacts using radical-oxynitridation-formed SiOxNy barrier for Si-based spin transistors, J. Electron. Mater. 41 (5) (2012) 954–958.
- [34] J. L. Cheng, M.W. Wu, J. Fabian, Theory of the spin relaxation of conduction electrons in silicon, Phys. Rev. Lett. 104 (2010) 016601.
- [35] P. Li, H. Dery, Spin-orbit symmetries of conduction electrons in silicon, Phys. Rev. Lett. 107 (2011) 107203.
- [36] Y. Song, H. Dery, Analysis of phonon-induced spin relaxation processes in silicon, Phys. Rev. B 86 (2012) 085201.
- [37] J. Li, L. Qing, H. Dery, I. Appelbaum, Field-induced negative differential spin lifetime in silicon, Phys. Rev. Lett. 108 (2012) 157201.
- [38] J. Li, I. Appelbaum, Modeling spin transport in electrostatically-gated lateral-channel silicon devices: Role of interfacial spin relaxation, *Phys. Rev. B* 84 (2011) 165318.
- [39] J. Li, I. Appelbaum, Lateral spin transport through bulk silicon, Appl. Phys. Lett. 100 (16) (2012) 162408.
- [40] G. L. Bir, G. E. Pikus, Symmetry and Strain-induced Effects in Semiconductors, John Willey & Sons, New York-Toronto, 1974.
- [41] D. Osintsev, O. Baumgartner, Z. Stanojevic, V. Sverdlov, S. Selberherr, Subband splitting and surface roughness induced spin relaxation in (001) silicon SOI MOSFETs, *Solid-State Electron*. 90 (2013) 34–38.
- [42] V. Sverdlov, Strain-Induced E\_ects in Advanced MOSFETs, Springer, Wien—New York, 2011.
- [43] M. V. Fischetti, Z. Ren, P. M. Solomon, M. Yang, K. Rim, Six-band k-p calculation of the hole mobility in silicon inversion layers: Dependence on surface orientation, strain, and silicon thickness, *J. Appl. Phys.* 94 (2) (2003) 1079–1095.
- [44] M.V. Fischetti, S. E. Laux, Monte Carlo study of electron transport in silicon inversion layers, Phys. Rev. B 48 (4) (1993) 2244–2274.
- [45] D. Osintsev, Modeling spintronic effects in silicon, Dissertation, Institute for Microelectronics, TU Wien (2014).
- [46] Y. Bychkov, E. Rashba, Properties of a 2D electron gas with lifted spectral degeneracy, JETP Lett. 39 (2) (1984) 78-81.
- [47] S. Giglberger, L. E. Golub, V. V. Bel'kov, S. N. Danilov, D. Schuh, C. Gerl, F. Rohlfing, J. Stahl, W. Wegscheider, D. Weiss, W. Prettl, S. D. Ganichev, Rashba and Dresselhaus spin splittings in semiconductor quantum wells measured by spin photocurrents, *Phys. Rev. B* 75 (2007) 035327.
- [48] J.-M. Jancu, J.-C. Girard, M. O. Nestoklon, A. Lemaître, F. Glas, Z. Z. Wang, P. Voisin, Electric field effect on electron spin splitting in SiGe/Si quantum wells, *Phys. Rev. B* 77 (2008) 155328.

[49] M. Prada, G. Klimeck, R. Joynt, Spin-orbit splittings in Si/SiGe quantum wells: From ideal Si membranes to realistic heterostructures, *New Journal of Physics* 13 (1) (2011) 013009.

[50] Z. Wilamowski, W. Jantsch, Suppression of spin relaxation of conduction electrons by cyclotron motion, Phys. Rev. B 69 (2004) 035328.